ACS OMEGA

Article

Cite This: ACS Omega 2018, 3, 17188−17198

http://pubs.acs.org/journal/acsodf

Characterization of the Evolution of Crystallization Fouling in Membranes

Adesola Oluwasijibomi Olufade* and Carey James Simonson

Department of Mechanical Engineering, University of Saskatchewan, 57 Campus Drive, Saskatoon, Saskatchewan S7N 5A9, Canada

ABSTRACT: Liquid-to-air membrane energy exchangers (LAMEEs) are promising in heating, ventilating, and air-conditioning applications because they are able to use semipermeable membranes to transfer heat and moisture between air and liquid desiccant streams. However, the development of crystallization fouling in membranes may pose a great risk to the long-term performance of LAMEEs. The main aim of this paper is to characterize the evolution of crystallization fouling in membranes through the use of both noninvasive and invasive methods. Noninvasive methods are used to study the development of fouling in the LAMEE by monitoring the changes in moisture flux through the membrane and overall moisture-transfer resistance of the LAMEE. On the other hand, invasive methods are implemented to characterize fouled membranes by using optical microscopy and scanning electron microscopy (SEM) to depict the morphology of crystal deposits and energy-dispersive X-ray spectroscopy (EDX) to identify the composition of the deposits. Experiments are performed by using air to dehydrate $MgCl_2$(aq) at two operating conditions of low and high fouling rates. The results show that the moisture flux decreases and the moisture-transfer resistance increases more considerably during the test at the high fouling rate than in the test at the low fouling rate. SEM micrographs show that cake crystal deposits cover the membrane surface in the test at the high fouling rate, whereas only few crystal particles are observed on the membrane in the test at the low fouling rate. Furthermore, the crystal deposits undergo more structural changes in the tests at the high fouling rate than in the tests at the low fouling rate, possibly because of the higher moisture transfer rate through the membrane in the tests at the high fouling rate. Finally, the SEM−EDX analysis confirms that the crystal deposits primarily consist of Mg, Cl, and O elements.

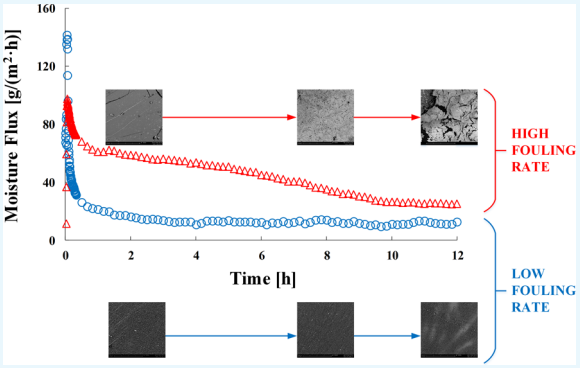

1. INTRODUCTION

1.1. Motivation. Fouling can be defined as the amassing and attachment of unwanted matter to surfaces, such as in heat exchangers[1] or membranes.[2] Fouling affects over 90% of industrial heat exchangers[3] and degrades the overall heat-transfer coefficient[4] and effectiveness[5] of heat exchangers because of the additional resistance to heat transfer caused by the buildup of deposits on surfaces. Fouling can also reduce the quantity of fluid that passes through membranes when substances are deposited internally within the pores of membranes or externally on membrane surfaces.[2]

Fouling results in extra energy consumption and costs due to overdesigned exchangers, cleaning, maintenance, and production losses.[3,6−10] The increase in energy and material consumption caused by fouling leads to an increase in the amount of CO_2 emissions released into the environment and reduces the sustainability of industrial processes. For instance, a 300 μm-thick fouling layer in the condenser of a power plant reportedly increased CO_2 emissions by 23 tons per day.[11] In addition, it has been estimated that fouling in crude oil refineries worldwide accounts for about 2.5% of the global CO_2 emissions caused by humans.[12]

Fouling has a significant impact on the economy of industries and nations. A 30−40% increase in the area of a heat exchanger because of fouling can increase the capital cost of the exchanger by 25%.[13] Xu et al.[6] conducted an economic evaluation of a coal-fired power plant in China in 2000 and found that fouling resulted in a 29% increase in heat-transfer surface area. A recent estimate of the national economic cost of fouling reported that heat exchanger fouling costs 0.25−0.35% of the gross national product of industrialized countries.[14] Consequently, in 2016, fouling accounts for up to US$ 6 billion in Canada and US$ 66 billion in the USA based on data from The World Bank Group.[15,16] It should be noted that the costs associated with fouling may be higher for a rapidly developing nation like China because of the substantial market demand[14] and high rate of industrialization in the country.

1.2. Fouling Detection Methods. Several methods are used to detect and monitor fouling in heat and membrane exchangers. These fouling detection methods can be broadly categorized into noninvasive and invasive methods. Invasive methods interrupt the operation of equipment to inspect the existence of fouling and are unsuitable for real-time inspection of exchangers. However, noninvasive methods can be used to

Received: May 18, 2018
Accepted: September 11, 2018
Published: December 13, 2018

DOI: 10.1021/acsomega.8b01058
ACS Omega 2018, 3, 17188−17198

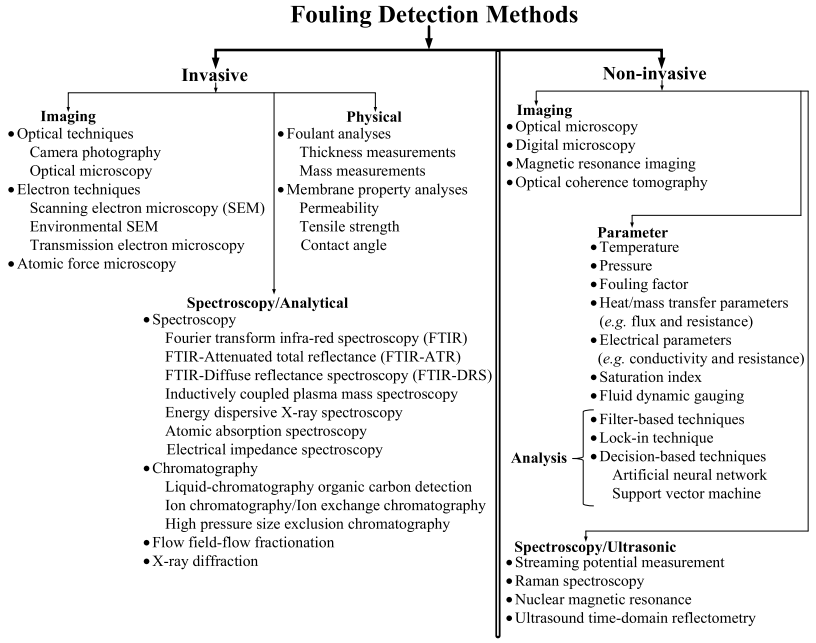

Figure 1. Classification of fouling detection methods. Note: The methods are compiled from refs.[7,11,17−58]

detect fouling without disrupting processes and are useful for real-time monitoring of fouling growth. An overview of fouling detection methods is shown in Figure 1.

Figure 1 shows various noninvasive and invasive methods, which are further divided into subcategories that include lists of specific methods. As an example, scanning electron microscopy (SEM) is an invasive method that is classified under the "imaging" subcategory because it can be used to image the surface of a material to detect the presence of fouling deposits. Experimental measurements (such as moisture flux or temperature) are noninvasive methods that are placed under the "parameter" subcategory. Parameters can be used to indirectly detect or monitor fouling because they indicate the impact of deposit accumulation on the performance of exchangers. Decision-based techniques are another example of noninvasive methods. Decision-based techniques are classified under the "analysis" subcategory and can be used to detect fouling by analyzing process parameters (e.g., moisture flux).

1.3. Research Gaps. This paper addresses the limited application of noninvasive and invasive methods to systematically identify the evolution of: (i) fouling in heat and membrane exchangers for diverse applications and (ii) crystallization fouling in membrane exchangers for heating, ventilating, and air-conditioning (HVAC) applications.

1.3.1. Fouling in Heat and Membrane Exchangers in Diverse Applications. Few studies have used both noninvasive and invasive methods to characterize the evolution of fouling.[42,59] However, many studies have used only noninvasive methods to observe how fouling evolves,[37,40,46,49,52,53,60−62] and some of these studies[37,46,49] subsequently used invasive methods (e.g., SEM) to characterize the morphology of fouling deposits after a test (and not during the test).

Although noninvasive methods can be used for real-time observation of fouling, they do not provide information on how the boundary conditions at the membrane interface affect the morphological transformations of the fouling deposits. Consequently, both noninvasive and invasive methods are needed to thoroughly understand the evolution of fouling in membranes. The application of both noninvasive and invasive methods to study the evolution of fouling is systematically pursued in this paper.

1.3.2. Crystallization Fouling in Membrane Exchangers for HVAC Applications. This paper also focuses on fouling in membrane-based exchangers for HVAC applications. This is because membranes are progressively gaining acceptance in HVAC technologies, e.g., air-to-air membrane energy recovery ventilators.[63,64] In addition, membranes can potentially reduce the energy consumption of HVAC equipment,[63] and HVAC systems consume about half of the energy used in buildings and one-fifth of the total energy produced in developed countries.[65]

The membrane exchanger studied in this paper is called a liquid-to-air membrane energy exchanger (LAMEE). Unlike conventional heat exchangers that can only transfer heat between fluid streams, the LAMEE can transfer heat and moisture between air and liquid desiccant streams using a semipermeable membrane.[66−68] However, crystals may precipitate from the desiccant solution and accumulate within the membrane and degrade the performance of the LAMEE.[69]

In a recent study by the authors,[69] the rate of moisture transfer through the membrane was identified as a key parameter that influences the likelihood of crystallization fouling in LAMEEs. However, the effect of moisture-transfer rate on the evolution of crystallization fouling in membranes was not assessed in the same study.[69] In addition, the papers on crystallization fouling in LAMEEs[27,49,69] have neither methodically identified the changes in the morphology of deposits during a fouling test nor determined the composition of deposits on fouled membranes.

1.4. Research Objectives. The main aim of this paper is to characterize the evolution of crystallization fouling in membranes. The specific objectives of this paper are to

1. Identify the evolution of crystallization fouling in membranes using noninvasive and invasive methods.

DOI: 10.1021/acsomega.8b01058
ACS Omega 2018, 3, 17188−17198

2. Identify the composition and structure of deposits on membranes using invasive methods.

2. THEORETICAL BACKGROUND

Crystallization fouling primarily involves the precipitation of ions from a salt solution and subsequent attachment to a surface.[70] Crystallization fouling is frequently encountered in industrial processes and is also known as scaling[70] or encrustation,[71] because it sometimes results in the attachment of precipitates to surfaces. The mechanisms of crystallization fouling kinetics are influenced by several interrelated parameters.[71,72] Some parameters that influence crystallization fouling include the properties of solutions (concentration, pH), bulk and surface fluids (temperature, velocity), and materials (roughness, surface energy).[2,14,48,73,74]

2.1. Mechanisms of Crystallization Fouling. The primary condition for crystallization is the supersaturation of an aqueous solution.[14,73,75] The supersaturation of a solution can be achieved by diverse means, including evaporating a solution above its saturation concentration, cooling a normally soluble solution below its saturation temperature or heating an inversely soluble solution above its saturation temperature, modifying the pH of a solution, and mixing solutions that can precipitate their ions.[76−78] Although supersaturation is an essential requirement, it does not inevitably lead to crystallization.[14]

The supersaturation of an aqueous solution may be succeeded by nucleation. Nucleation can be classified into primary or secondary types,[77] and primary nucleation can either be homogenous or heterogeneous. Homogenous nucleation involves the spontaneous formation of nuclei in a supersaturated solution without the presence of foreign particles or surface defects, whereas heterogeneous nucleation is often triggered by the presence of surface imperfections or impurities in a solution.[14,77] Bott suggested that heterogeneous nucleation is more likely to be the cause of crystallization fouling in heat exchangers in the industry,[77] possibly because the total change in free energy required for heterogeneous nucleation is less than that of homogenous nucleation.[75] Secondary nucleation is initiated by seeded crystals in a solution, as opposed to primary nucleation which does not require the presence of crystals to occur.[75]

Nuclei can begin to grow if they exceed their critical size after nucleation.[75] Crystal growth can be explained by three main theories based on surface energy, adsorption layer, and diffusion.[77] The surface energy theory postulates that the lowest surface energy controls the development of crystals, whereas the adsorption layer theory suggests that the crystal growth is intermittent and takes place by the buildup of crystal layers.[77] However, the diffusion theory is often applied to explain crystal growth in heat exchanger fouling.[72,76,77,79] The diffusion theory states that the development of crystals may be primarily controlled by diffusion mass transfer, surface reaction integration, or a combination of both mechanisms depending on the operating condition.[72] Mass diffusion is driven by the difference between the bulk and interface concentrations, whereas surface reaction integration is controlled by difference between the saturation and interface concentrations.[77]

2.2. Crystallization Fouling in a LAMEE. As previously stated, a LAMEE is a liquid-to-air membrane exchanger which can be used to condition the temperature and humidity of an air stream without direct contact between the air stream and the liquid desiccant. During the operation of a LAMEE, the operating condition may favor the seeding of crystals in the liquid desiccant, and the crystals may block the membrane pores or form a layer on the membrane surface. Figure 2 shows the possible mechanisms of the development of crystallization fouling in a LAMEE during the dehydration of a liquid desiccant solution.

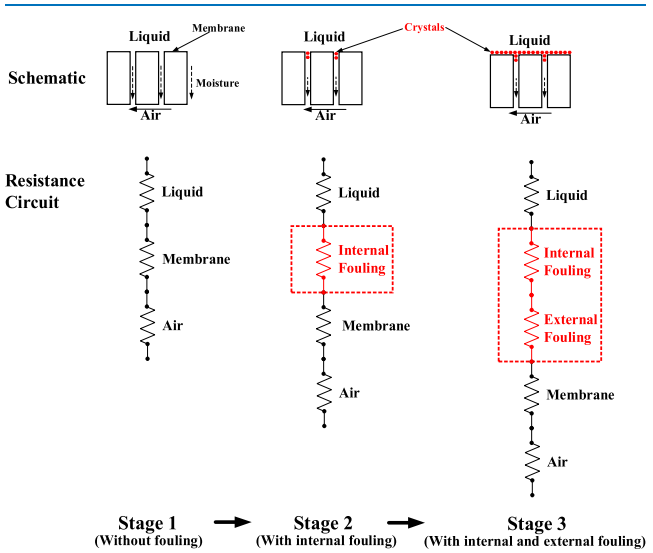

Figure 2. Development of crystallization fouling in a LAMEE (adapted from ref 80).

In Figure 2, the first phase is stage 1. Stage 1 depicts the operation of a LAMEE without the presence of fouling. As air flows on one side of the LAMEE, the difference in the water vapor concentration (humidity ratio) between the air and solution sides initiates the evaporation of water from the desiccant solution. Afterward, moisture diffuses through the membrane pores into the air stream. In Figure 2, stage 1 is also shown in the form of a resistance circuit, in which the LAMEE consists of liquid-side, membrane, and air-side moisture-transfer resistances.

The LAMEE may progress to stage 2 as moisture continuously evaporates from the desiccant solution, and the solution concentration increases until supersaturation occurs at the solution−membrane interface. Crystals may directly nucleate inside the membrane pores and obstruct the permeation of moisture through the membrane. In stage 2, a resistance is added to the LAMEE because of internal fouling from crystals that accumulate in the membrane pores.

It is possible for the growth of crystals in the LAMEE to reach stage 3, where crystals agglomerate and form a cake layer on the membrane surface. The formation of crystal cakes on the membrane surface is known as external fouling because the deposits accumulate on the membrane surface and are not lodged within the pores. Furthermore, a high rate of crystal development may shorten the phase of internal fouling in stage 2 and rapidly evolve into external fouling in stage 3. However, internal fouling does not necessarily lead to external fouling, and both mechanisms may occur either independently or simultaneously. In stage 3, the LAMEE consists of two additional resistances from internal and external fouling.

The presence of fouling in the LAMEE at stage 2 (internal fouling) and stage 3 (internal and external fouling) is expected to reduce the moisture flux through the membrane and

DOI: 10.1021/acsomega.8b01058
ACS Omega 2018, 3, 17188−17198

increase the overall moisture-transfer resistance of the LAMEE. It should be noted that the development of crystallization fouling along the vertical cross section of a membrane as described in stages 2 and 3 are provided for description purposes and will not be examined in this paper.

3. METHODOLOGY

In this section, a test facility that is developed to test crystallization fouling in LAMEEs is first presented (Section 3.1). Second, the properties of the membrane used in the LAMEE are highlighted (Section 3.2). Third, the noninvasive and invasive methods that are used to characterize the evolution of crystallization fouling in membranes are presented in Sections 3.3 and 3.4, respectively.

3.1. Test Facility. A test facility is constructed to test the LAMEE under different operating conditions in order to examine the development of crystallization fouling in membranes. The LAMEE uses an air stream with a lower moisture content to dehydrate a stationary liquid desiccant solution. As previously explained (see Section 2.2), the continuous removal of moisture from the liquid desiccant can lead to crystallization fouling in the membrane. A schematic of the complete test facility is shown in Figure 3.

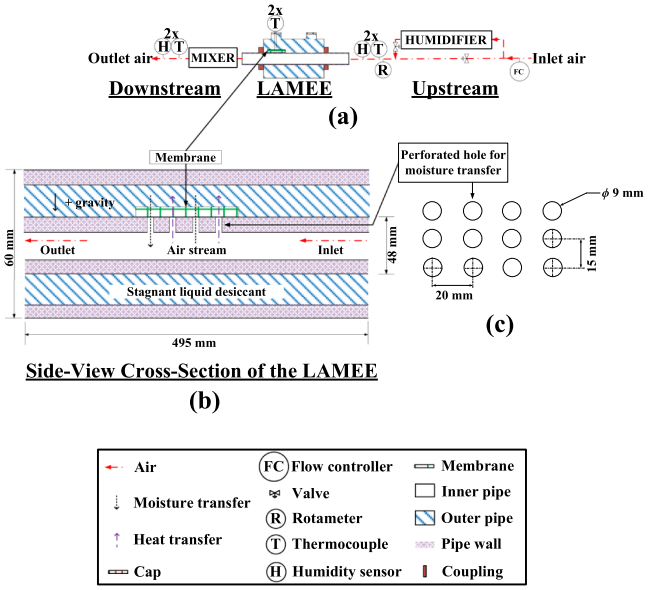

Figure 3. Schematic of the test facility.[69] Note: The schematic consists of the (a) upstream section, LAMEE, and downstream section of the test facility, (b) side-view cross-section of the LAMEE, and (c) arrangement of perforated holes on the inner pipe of the LAMEE. The diagrams are not drawn to scale.

Figure 3 shows (a) an overview of the test facility (upstream section, LAMEE, and downstream section), (b) side-view cross section of the LAMEE, and (c) configuration of holes on the inner pipe of the LAMEE. The pipes that are used to construct the LAMEE are impermeable to moisture transfer. Therefore, holes are drilled into the inner pipe of the LAMEE to facilitate the exchange of moisture between the air stream and desiccant solution (see Figure 3c). The operational procedure of the test facility and the details of its instrumentation, uncertainty analysis, and mass and energy balances are documented in ref 69.

The test facility can be used to test crystallization fouling in the LAMEE under different operating conditions by varying the air relative humidity and solution concentration. In this paper, fouling is studied under two operating conditions that are presented in Table 1.

Table 1. Test Operating Conditions

parameter and unit	condition 1 (high fouling rate)	condition 2 (low fouling rate)
relative humidity of air, RHair [%]	10 ± 1	30 ± 2
dimensionless solution concentration, C^*_{sol}[a] [-]	~1.03 (supersaturated)	~1.0 (saturated)
temperature of air and desiccant solution [°C]	23 ± 2	

[a]Csol* is the ratio of the concentration of a desiccant solution to its saturated concentration.

In Table 1, Condition 1 has a higher fouling rate than Condition 2. This is because the moisture-transfer rate is higher for Condition 1 because the air stream is at a lower relative humidity (RH_{air} = 10%) compared with Condition 2 where RH_{air} = 30%. In addition, Condition 1 involves the use of supersaturated solution (Csol* = 1.03) which raises the propensity for a higher rate of crystallization within the bulk solution than Condition 2 where the solution is only saturated (Csol* = 1.0).

Experimental tests are performed at different time intervals that range from 30 min to 12 h, and repeated at certain time intervals to ensure measurement repeatability.

3.2. Membrane. The membrane is perhaps the most essential component of a LAMEE[67] because it preferentially allows the passage of water vapor between the air and solution. The membranes used in HVAC systems are usually polymer-based,[63,81] and either porous or nonporous.[81] The micrographs of the membrane that is used in the LAMEE in this paper is shown in Figure 4.

Figure 4a shows images of a membrane which consists of a polytetrafluoroethylene (PTFE) support structure and expanded PTFE surface layer. The support structure provides a strong backing for the membrane,[63] whereas the surface layer is hydrophobic and serves to prevent liquid from permeating through the membrane. A close-up image of the membrane surface is shown in Figure 4b, and it comprises interwoven PTFE fibers and numerous stretched pores. The pores are the areas where moisture diffuses through the membrane.

Two important properties of membranes used in LAMEEs are vapor diffusion resistance (VDR) and liquid penetration pressure (LPP).[82] Membranes with low VDR are desirable because they have a high permeability to moisture transfer. Furthermore, the LPP of a membrane should be sufficiently high to overcome the pressure exerted on the membrane and prevent wetting. Although the VDR of a membrane can be reduced by increasing the pore sizes and reducing the thickness, this could result in the reduction of the membrane LPP.[63] Thus, a membrane with an appropriate pore size should be selected to guarantee a low VDR and high LPP.[63,67] The properties of the membrane used in this paper are given in Table 2.

After each experimental test, the membrane is detached from the LAMEE and preserved in a sterilized desiccator at room temperature (~24 °C). This is done to ensure that crystals that may have formed within the membrane do not absorb

DOI: 10.1021/acsomega.8b01058
ACS Omega 2018, 3, 17188−17198

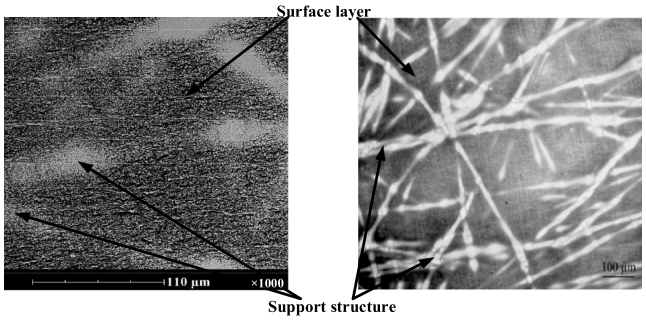

(a) Membrane surface layer and support structure.

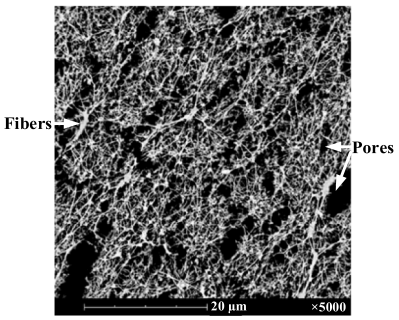

(b) Membrane surface layer.

Figure 4. Micrographs of the membrane used in the LAMEE. Note: The image on the right hand side of (a) was taken with an optical microscope, whereas the images in (b) and the left hand side of (a) were taken with a scanning electron microscope. The optical microscopy and SEM methods are described in Sections 3.4.1 and 3.4.2, respectively.

Table 2. Properties of the Membrane Used in the LAMEE[82] (Adapted from ref 69)[a]

parameter and unit	value
material [-]	expanded PTFE laminates
pore size [μm]	0.3
porosity [%]	85
VDR [s/m]	97 ± 11
thickness [μm]	540 ± 16
LPP [kPa]	>82

[a]The micrographs of the membrane are shown in Figure 4.

moisture from the environment and dissolve. The sections of a membrane that are subsequently analyzed are those that overlay on the holes in the inner pipe of the LAMEE where moisture transfer occurs (see Figure 3c).

3.3. Noninvasive Methods. Noninvasive methods are used to delineate the evolution of crystallization fouling by monitoring the performance parameters of the LAMEE. These performance parameters are calculated from in situ experimental measurements and are namely moisture flux and moisture-transfer resistance.

The moisture flux, $\dot{m}''_v$, represents the rate of mass of water vapor that permeates from the desiccant solution to the air stream per unit surface area of the membrane, and is given by

$$\dot{m}''_v = \frac{\dot{m}_{air}(W_{air,out} - W_{air,in})}{A_{mem}} \quad (1)$$

The moisture-transfer resistance of the LAMEE, R, is the overall resistance to moisture transfer between the air and solution sides, as given by

$$R = \frac{\Delta W_{lm}}{\dot{m}''_v} \quad (2)$$

The log-mean humidity ratio, ΔW_{lm}, is given by

$$\Delta W_{lm} = \frac{(W_{sol} - W_{air,in}) - (W_{sol} - W_{air,out})}{\ln\left(\frac{W_{sol} - W_{air,in}}{W_{sol} - W_{air,out}}\right)} \quad (3)$$

The change in the concentration of the desiccant solution (before and after a test) is negligible for all the tests conducted. Therefore, eq 3 can be simplified into

$$\Delta W_{lm} = \frac{W_{air,out} - W_{air,in}}{\ln\left(\frac{W_{sol} - W_{air,in}}{W_{sol} - W_{air,out}}\right)} \quad (4)$$

3.4. Invasive Methods. In this paper, three invasive methods are used to characterize the buildup of deposits on a membrane surface ex situ. The three methods are optical microscopy, SEM, and energy dispersive X-ray spectroscopy (EDX) and have been widely used to study fouling in several studies (see review papers[22,55]).

3.4.1. Optical Microscopy. Optical microscopy involves the use of lenses to magnify transmitted or reflected light from a surface and has been described as the most direct way to monitor fouling on a membrane.[22] Although optical microscopy instruments are affordable and time-saving, they are limited by their need for a lucid fluid medium.[25] In addition, optical microscopy is typically used in ambient environments which are not conducive for the preservation of hygroscopic crystals that may be deposited in membranes. Notwithstanding, optical microscopy is used in this paper as a preliminary technique to confirm the presence of crystal particles on a fouled membrane.

A fresh membrane and a supposedly fouled membrane are selected for imaging. The membrane samples are removed from the desiccator, firmly taped to a microscope slide, and examined with a Zeiss AxioPlan microscope. The image processing program of the microscope[83] is used to improve the contrast of the images to clarify and intensify the features on the membrane surface. A comparison of the images of fresh and fouled membranes is shown in Figure 5.

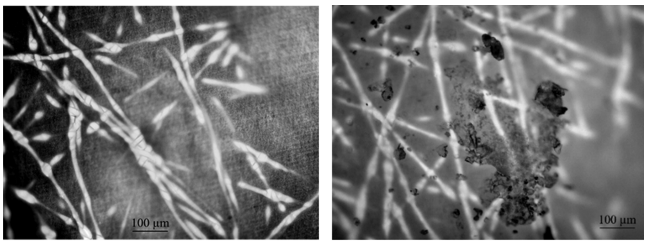

(a) Fresh membrane (b) Fouled membrane.

Figure 5. Comparison of the surface sections of (a) fresh and (b) fouled membranes from a 30 min test at the high fouling rate (RH_{air} = 10%, Csol* = 1.03).

Figure 5a clearly shows the surface layer and support structures of the fresh membrane (see Figure 4a), whereas crystals are clearly visible as dark particles on the fouled membrane image in Figure 5b. The images in Figure 5b not only confirm the formation of crystal particles on the membrane surface but also demonstrate that there was such

DOI: 10.1021/acsomega.8b01058
ACS Omega 2018, 3, 17188−17198

a rapid and severe fouling that the crystals formed a cake structure within a 30 min period.

3.4.2. Scanning Electron Microscopy. SEM is a widely used surface characterization technique, which involves the bombardment of a surface with powerful electrons and subsequent detection/image reconstruction of the reflected or scattered electrons with electro-magnetic lenses.[22] SEM does not require the preparation of very thin samples like in transmission electron microscopy and can typically achieve a resolution of 1−10 nm which exceeds the limit of optical microscopy.[84] However, polymer membranes need to be coated with a conductive metal before SEM analysis to increase the conductivity of the membrane surface and resolution of the images obtained.[22,55]

In this paper, SEM is used to depict the morphological changes in the development of crystallization fouling on a membrane. Before imaging is performed, a preserved membrane is extracted from the desiccator and several sections of the membrane sample are dissected, mounted on stubs, and coated with a thin film of gold using an Edwards S150B gold sputter coater. SEM imaging is mostly done using a Phenom G2 Pure desktop scanning electron microscope with a resolution of 30 nm. However, the shapes of full-grown crystals on fouled membranes are imaged using a Hitachi SU8010 field emission scanning electron microscope which can achieve a resolution of 1.0−1.3 nm. SEM analysis is performed on membrane sections that are overlaid on the holes in the inner pipe of the LAMEE where moisture transfer occurs. For each test performed, several sections of a membrane are analyzed with the scanning electron microscope to assess the similarity of the crystal deposits.

Figure 6 shows some SEM images of different sections of fouled membranes.

Figure 6 shows that the crystals appear in the form of cake layers on the membrane surface. In addition, it can also be observed that the cake layers are fractured. The images from different sections of the membranes in Figure 6 confirm that the structure of the crystal particles is consistent across various sections of a membrane from repeated tests. Similar findings were also obtained for repeated tests at other operating conditions and time intervals.

3.4.3. Energy Dispersive X-ray Spectroscopy. EDX involves the use of a semiconductor component to analyze the electromagnetic energy reflected from a substance to determine the atomic composition of the substance.[55,84] EDX machines are typically used in conjunction with scanning electron microscopes or transmission electron microscopes[55] and are effective for identifying the elemental composition of fouling deposits in membranes.[46,55]

In this paper, an Oxford Instruments X-Max^N 50 mm^2 EDX machine is used in combination with a Hitachi SU6600 field emission scanning electron microscope to analyze the composition of deposits on a fouled membrane sample. The EDX method is hereby used to qualitatively identify the composition of crystal deposits observed in the SEM images of fouled membranes rather than to quantify the composition of the deposits.

4. RESULTS AND DISCUSSION

In this section, the noninvasive and invasive methods presented in Section 3 are used to address the objectives of this paper (i.e., to identify the evolution of crystallization fouling in membranes and identify the composition and structure of the fouling deposits).

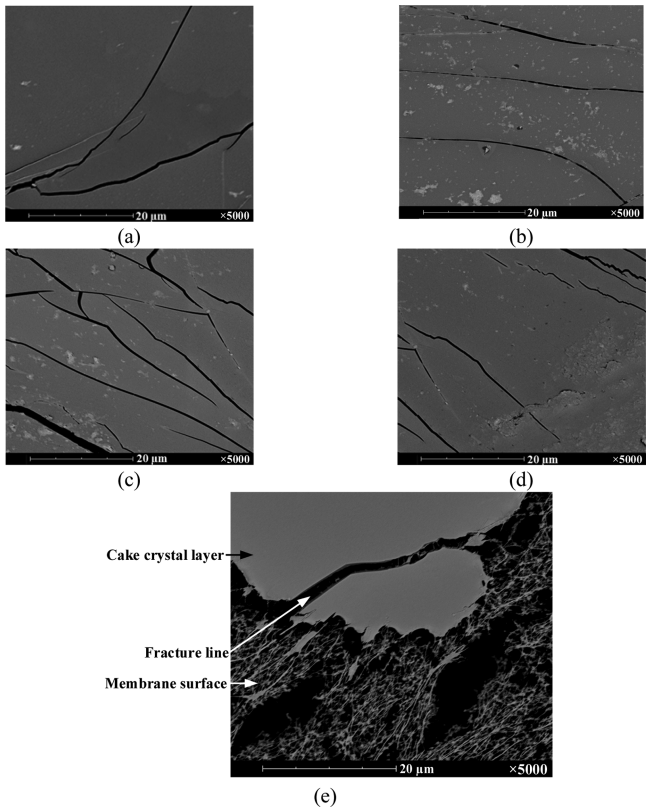

Figure 6. SEM micrographs of the surface sections of membranes after 2 h tests at the high fouling rate (RH_{air} = 10%, Csol* = 1.03). Note: Images from a first test at different locations of the membrane are shown in (a,b), while those from repeated tests are shown in (c−e).

4.1. Evolution of Fouling. *4.1.1. Noninvasive Methods (Moisture Flux and Moisture-Transfer Resistance).* Figure 7 depicts the evolution of fouling in a LAMEE at two operating conditions of low and high fouling rates, using both the moisture flux and moisture-transfer resistance parameters.

Figure 7a shows a comparison of the evolution of moisture flux through the membrane during the tests at the low and high fouling rates. It can be seen that there is an initial overshoot of the moisture flux at the start of the test at the low fouling rate. Afterward, the moisture flux continuously decays during the entire duration of both tests. Expectedly, the moisture flux is higher for the test at the high fouling rate compared with the test at the low fouling rate. However, the higher rate of moisture transfer in the test at the high fouling rate resulted in the considerable development of crystallization fouling in the LAMEE. The crystals possibly blocked the membrane pores and formed a layer on the membrane surface, thereby drastically impeding the permeation of moisture through the membrane. The slight decay in moisture flux in the test at the low fouling rate may be attributed to a minimal buildup of deposits on the membrane surface. The moisture flux decays and reaches quasi-steady-state conditions at ∼4 h for the test at the low fouling rate, whereas the moisture flux begins to flatten out at ∼11 h for the test at the high fouling rate.

Figure 7b shows that the moisture-transfer resistances of the LAMEE at the low and high fouling rates are at a similar magnitude at the start of the tests. The moisture-transfer

DOI: 10.1021/acsomega.8b01058
ACS Omega 2018, 3, 17188−17198

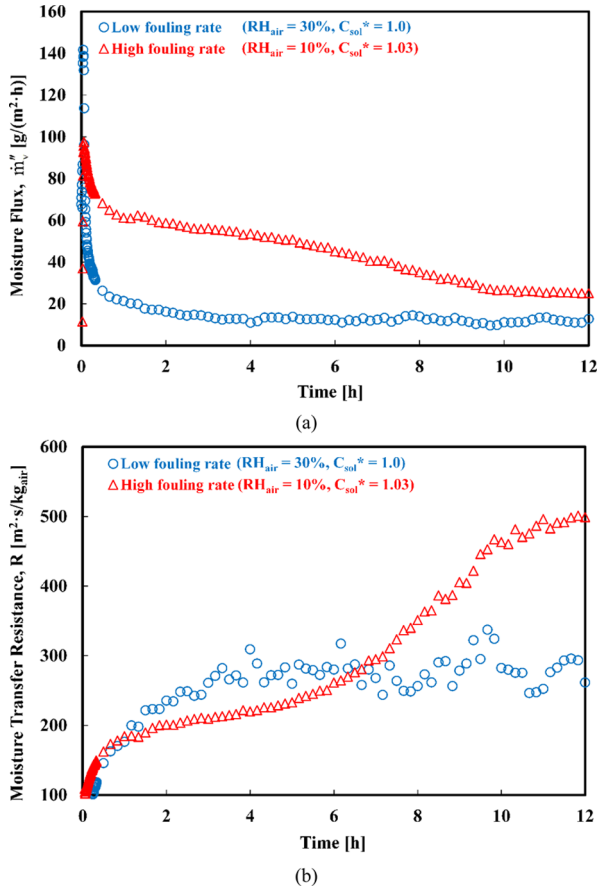

Figure 7. Evolution of crystallization fouling in the LAMEE using (a) moisture flux and (b) moisture-transfer resistance parameters for tests at the low and high fouling rates.

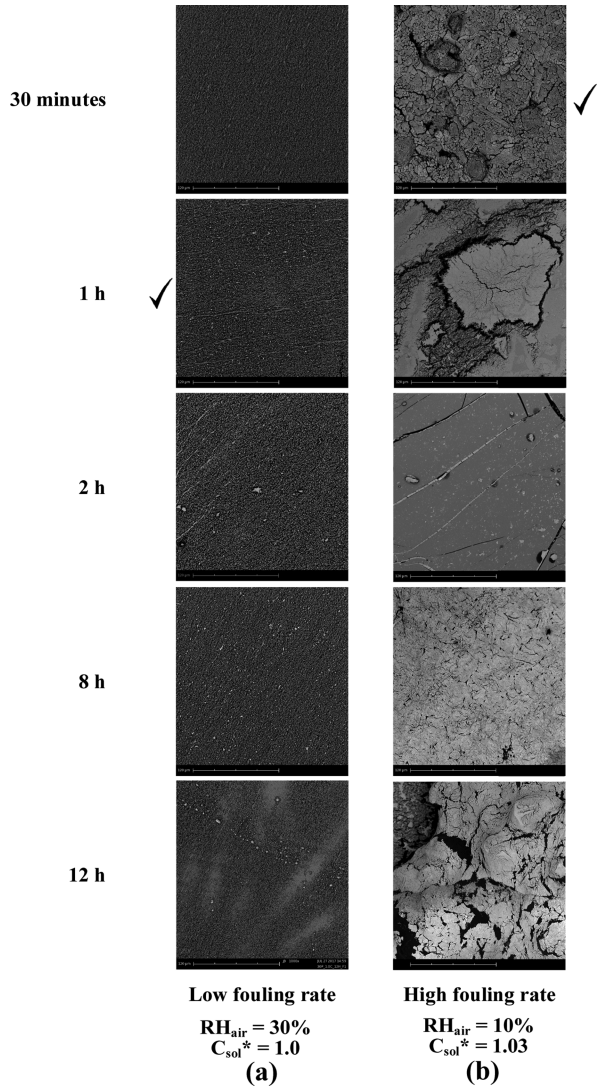

Figure 8. Evolution of crystallization fouling in membranes using the SEM method for tests performed at the (a) low and (b) high fouling rates. Note: The time that crystals are first observed on a membrane is indicated by a check mark that is adjacent to the corresponding membrane image. All the images are taken at a magnification of 1000 and the scale bars are 120 μm in length.

resistance for the test at the low fouling rate rises and attains quasi-steady-state conditions early at ∼4 h. For the test at the low fouling rate, the intermittent rise and fall in the moisture-transfer resistance can be attributed to (i) periodic changes (∼±1%) in the relative humidity of air supplied to the LAMEE and (ii) low driving force for moisture transfer between the desiccant solution and air stream (see eq 3). For the test at the high fouling rate, the moisture-transfer resistance substantially increases during the main part of the test and approaches an asymptotic limit toward the end of the test.

The results of the noninvasive methods in Figure 7 confirm that crystallization fouling in the LAMEE reduces the moisture flux through the membrane and increases the overall moisture-transfer resistance of the LAMEE (see Section 2.2).

4.1.2. Invasive Method (SEM). Figure 8 shows the SEM micrographs of membranes for tests performed at different intervals.

Figure 8 shows SEM micrographs that depict the evolution of crystallization fouling in membranes. The structural changes in the crystal deposits in Figure 8 are described in succeeding paragraphs.

In Figure 8a, crystal particles are not observed on the membrane surface within the first 30 min. A slow development of minute crystals is first seen at 1 h (denoted by a check symbol that is adjacent to the corresponding image); thereafter, there is negligible change in the structure or distribution of the particles even at 12 h. Within 1−12 h, the crystals remain mostly small and speckled which suggests that there is a very low rate of deposit accumulation on the membrane surface rather than the agglomeration of large-size crystals or development of cake layers. Thus, minimal external fouling appears to be the dominant mechanism at the low fouling rate.

In Figure 8b, coarse loosely-structured rock-like crystal particles are observed within the first 30 min (denoted by a check symbol that is adjacent to the corresponding image), possibly because of the supersaturation of the bulk solution coupled with a high rate of moisture transfer through the membrane. At 1 h, several crystals had agglomerated into cake formations which can be seen on the membrane. It is interesting to observe that at the 2nd h, the crystals form into smooth and fractured cake layers (see Figure 6). The continuous dehydration of $MgCl_2$(aq) likely led to the drying of the crystals, which resulted in the fragmentation of the cake layer within 2−12 h.

The morphological transformation of the crystal particles on the membrane surface is more significant at the high fouling

DOI: 10.1021/acsomega.8b01058
ACS Omega 2018, 3, 17188−17198

rate (Figure 8b) than at the low fouling rate (Figure 8a). As mentioned in Section 2.2, it is highly probable that substantial external fouling is the governing mechanism at the high fouling rate. The SEM method is unable to confirm if crystals are deposited within the pores of fouled membranes (i.e., internal fouling) because the electron beam of the scanning electron microscope physically melts the PTFE fibers of the membrane when the imaging magnification is significantly increased. However, the SEM method is able to establish the presence of external fouling for the tests at both low and high fouling rates.

The results in Figures 7 and 8 strongly suggest that during the dehydration of desiccant solutions in LAMEEs, a high moisture flux increases the amount of crystals that amass on membranes. In addition, a high rate of moisture transfer through membranes can lead to considerable changes in the morphology of the crystal deposits.

4.2. Characterization of Fouling Deposits (SEM, EDX). The elemental composition of deposit formations on fouled membranes is analyzed to confirm that the deposits are made up of $MgCl_2{\cdot}6H_2O$ crystals. The fouling deposits are first assessed with SEM to visualize the shape of a fully grown crystal on a layer of agglomerated deposits (Figure 9), and the composition of the deposits is identified using SEM−EDX (Figure 10).

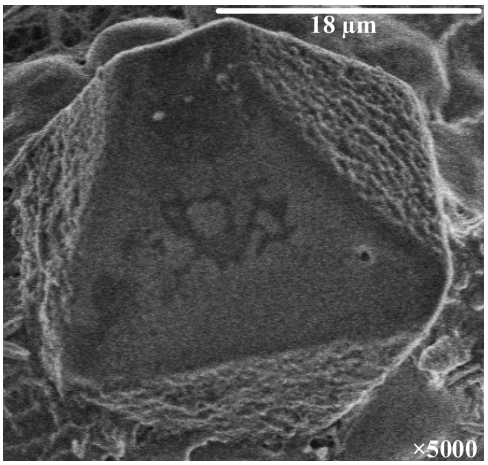

Figure 9. SEM micrograph of a crystal on a membrane after a 12 h test at the high fouling rate (RH_{air} = 10%, *Csol** = 1.03).

Figure 9 clearly depicts the octahedral shape of a $MgCl_2{\cdot}6H_2O$ crystal, which is consistent with what is reported in the literature.[85] On the other hand, Figure 10 depicts a section of a fouled membrane that completely overlays a perforated hole in the inner pipe (tube) of the LAMEE (see Figure 3c). The SEM image in Figure 10a shows a cake layer on the membrane, whereas the EDX plot in Figure 10b shows the elemental constituents of the cake layer. Expectedly, the highest peaks in Figure 10b correspond to Mg and Cl elements from $MgCl_2$. The O element in H_2O is detected but H is not detected because EDX is incapable of detecting hydrogen.[86,87] The presence of Au is detected because of the sputter coating of the membrane surface with gold. A low peak of C exists most likely because the membrane surface layer is made of C, whereas the low peaks of Ca may be attributed to the presence of trace quantities of $CaCO_3$ in H_2O(aq).

4.3. Comparison of Methods. A comparison of the noninvasive and invasive methods that are used to address the objectives of this paper is presented in Table 3.

Table 3. Comparison of the Noninvasive and Invasive Methods Implemented in This Paper[a]

	non-invasive methods		invasive methods		
factors	moisture flux/Moisture -transfer resistance		optical microscopy	SEM	EDX
practical application	non-invasive operation	++	−	−	−
	online/in situ monitoring	+	−	−	−
	financial affordability	++	−	−−	−
	space footprint constraints	++	−	−−	−
	installation and maintenance	++	−	−−	−
	sample preparation	++	−	−−	−−
operational features	direct detection	−	++	++	+
	sampling rate	++	−−	−−	−−
	calibration requirement	−	++	++	+
	computational demands	−	+	+	+
deposit analysis	morphology	−−	+	++	−−
	topology	−−	−	+	−−
	spatial resolution	−−	+	++	−
	composition	−−	−−	−−	++

[a] + = positive characteristic; ++ = very positive characteristic; − = negative characteristic; −− = very negative characteristic.

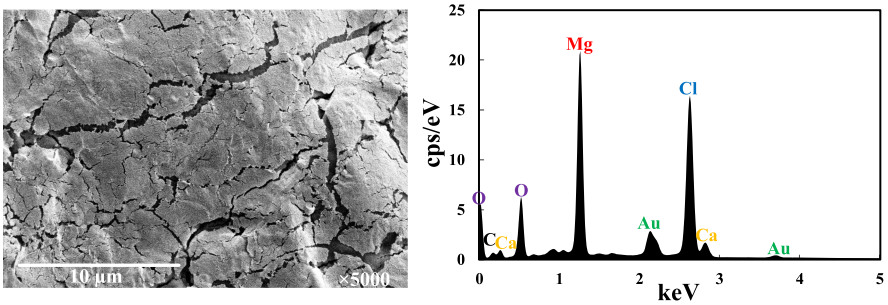

(a) SEM micrograph (b) EDX profile

Figure 10. (a) SEM micrograph and (b) corresponding EDX map profile of a membrane after a 12 h test at the high fouling rate (RH_{air} = 10%, *Csol** = 1.03). Note: The map profile in (b) corresponds to the area of the micrograph in (a). Note: cps = counts per second; eV = electron volts.

DOI: 10.1021/acsomega.8b01058
ACS Omega 2018, 3, 17188−17198

It can be seen from Table 3 that the main strength of the noninvasive methods is in their real-world applicability to detect and monitor fouling in operating exchangers, whereas the invasive methods are better suited to characterize fouling deposits. In addition, a comparison of the operational features of the noninvasive and invasive methods indicates that the noninvasive methods have an almost unlimited sampling rate but with a greater demand for data processing, whereas there is a practical limitation in the sampling rate of the invasive methods. Sampling rate refers to the frequency in which data can be collected and analyzed to study fouling.

5. CONCLUSION

The main aim of this paper is to characterize the evolution of crystallization fouling in membranes through the application of noninvasive and invasive methods. Membranes are fouled during 12 h tests in which $MgCl_2$(aq) is dehydrated in a LAMEE at two operating conditions of low and high fouling rates. The noninvasive methods consist of two parameters (moisture flux and moisture-transfer resistance) that are used to monitor the development of fouling in a LAMEE. The invasive methods consist of optical microscopy and SEM which are used to visualize the morphology of crystal deposits, and EDX which is used to identify the composition of the deposits.

The major findings from the paper are outlined as follows:

1. Crystallization fouling decreases the moisture flux through the membrane and increases the moisture-transfer resistance of the LAMEE more significantly in the test at the high fouling rate than in the test at the low fouling rate.
2. SEM micrographs show that cake crystal deposits are observed on membrane surfaces at the high fouling rate, whereas only few crystal particles are deposited on membranes at the low fouling rate.
3. The crystal deposits undergo greater structural transformations in tests performed at the high fouling rate compared with tests performed at the low fouling rate. The high rate of moisture transfer through the membrane is the likely reason for the substantial changes observed in crystal deposits at the high fouling rate.
4. The SEM micrograph of a crystal deposit on a membrane confirms the octahedral shape of $MgCl_2 \cdot 6H_2O$.
5. EDX analysis indicates that the crystal deposits compose of mainly Mg, Cl, and O elements.

AUTHOR INFORMATION

Corresponding Author

*E-mail: aoo021@mail.usask.ca.

ORCID

Adesola Oluwasijibomi Olufade: 0000-0003-4862-4173

Notes

The authors declare no competing financial interest.

ACKNOWLEDGMENTS

Adesola Olufade appreciates the financial support provided by the Dean's Scholarship, Toyota Automotive Engineering and Safety Scholarship, and Robert Falside Stoddart Memorial Scholarship at the University of Saskatchewan, and funding from the National Science and Engineering Research Council of Canada (NSERC).

NOMENCLATURE

Roman Symbols

A_{mem}, membrane surface area (m^2)
$\dot{m}$, mass flow rate (kg/s)
$\dot{m}''_v$, moisture flux ($g/(m^2 \cdot h)$)
R, moisture-transfer resistance ($m^2 \cdot s/kg_{air}$)
W, humidity ratio (kg_w/kg_{air})
ΔW_{lm}, log-mean humidity ratio (kg_w/kg_{air})

Subscripts

air, air
in, inlet of the LAMEE
out, outlet of the LAMEE
sol, salt solution
w, water vapor

REFERENCES

(1) Shah, R. K.; Sekulić, D. P. Fouling and Corrosion. *Fundamentals of Heat Exchanger Design*; John Wiley & Sons, Inc.: Hoboken, NJ, 2003; pp 863−905.

(2) Field, R. Fundamentals of Fouling. In *Membrane Technology*; Peinemann, K.-V., Ed.; Wiley-VCH Verlag GmbH & Co. KGaA: Weinheim, Germany, 2010; Vol. *4*, pp 1−23.

(3) Müller-Steinhagen, H. Heat transfer fouling: 50 years after the Kern and Seaton model. *Heat Transfer Eng.* **2011**, *32*, 1−13.

(4) Geddert, T.; Augustin, W.; Scholl, S. Induction time in crystallization fouling on heat transfer surfaces. *Chem. Eng. Technol.* **2011**, *34*, 1303−1310.

(5) Assis, B. C. G.; Lemos, J. C.; Liporace, F. S.; Oliveira, S. G.; Queiroz, E. M.; Pessoa, F. L. P.; Costa, A. L. H. Dynamic optimization of the flow rate distribution in heat exchanger networks for fouling mitigation. *Ind. Eng. Chem. Res.* **2015**, *54*, 6497−6507.

(6) Xu, Z. M.; Yang, S. R.; Guo, S. Q.; Zhao, H.; Qi, B.; Zhang, Z. B. Costs due to utility boiler fouling in China. *Heat Tran. Asian Res.* **2005**, *34*, 53−63.

(7) Shirazi, S.; Lin, C.-J.; Chen, D. Inorganic fouling of pressure-driven membrane processes - A critical review. *Desalination* **2010**, *250*, 236−248.

(8) Guo, W.; Ngo, H.-H.; Li, J. A mini-review on membrane fouling. *Bioresour. Technol.* **2012**, *122*, 27−34.

(9) Goosen, M. F. A.; Sablani, S. S.; Al-Hinai, H.; Al-Obeidani, S.; Al-Belushi, R.; Jackson, D. Fouling of reverse osmosis and ultrafiltration membranes: A critical review. *Sep. Sci. Technol.* **2005**, *39*, 2261−2297.

(10) Cheng, Y. H.; Chen, H. Y.; Zhu, Z. C.; Jen, T. C.; Peng, Y. X. Experimental study on the anti-fouling effects of Ni-Cu-P-PTFE deposit surface of heat exchangers. *Appl. Therm. Eng.* **2014**, *68*, 20−25.

(11) Gudmundsson, O.; Palsson, O. P.; Palsson, H.; Lalot, S. Online fouling detection of domestic hot water heat exchangers. *Heat Transfer Eng.* **2016**, *37*, 1231−1241.

(12) Müller-Steinhagen, H.; Malayeri, M. R.; Watkinson, A. P. Heat exchanger fouling: Environmental impacts. *Heat Transfer Eng.* **2009**, *30*, 773−776.

(13) Al Nasser, W. N.; Shah, U. V.; Nikiforou, K.; Petrou, P.; Heng, J. Y. Y. Effect of silica nanoparticles to prevent calcium carbonate scaling using an in situ turbidimetre. *Chem. Eng. Res. Des.* **2016**, *110*, 98−107.

(14) Zhao, X.; Chen, X. D. A Critical Review of Basic Crystallography to Salt Crystallization Fouling in Heat Exchangers. *Heat Transfer Eng.* **2013**, *34*, 719−732.

(15) The World Bank Group. GNI, PPP (current international $)—Canada http://data.worldbank.org/indicator/NY.GNP.MKTP.PP.CD?locations=CA (accessed Aug 3, 2017).

DOI: 10.1021/acsomega.8b01058
ACS Omega 2018, 3, 17188−17198

(16) The World Bank Group. GNI, PPP (current international $)—United States http://data.worldbank.org/indicator/NY.GNP.MKTP.PP.CD?locations=US (accessed Aug 8, 2017).
(17) Warsinger, D. M.; Swaminathan, J.; Guillen-Burrieza, E.; Arafat, H. A.; Lienhard V, J. H. Scaling and fouling in membrane distillation for desalination applications: A review. *Desalination* **2015**, *356*, 294−313.
(18) Sanmartino, J. A.; Khayet, M.; García-Payo, M. C.; El Bakouri, H.; Riaza, A. Desalination and concentration of saline aqueous solutions up to supersaturation by air gap membrane distillation and crystallization fouling. *Desalination* **2016**, *393*, 39−51.
(19) Shi, X.; Tal, G.; Hankins, N. P.; Gitis, V. Fouling and cleaning of ultrafiltration membranes: A review. *J. Water Process Eng.* **2014**, *1*, 121−138.
(20) Antony, A.; Low, J. H.; Gray, S.; Childress, A. E.; Le-Clech, P.; Leslie, G. Scale formation and control in high pressure membrane water treatment systems: A review. *J. Membr. Sci.* **2011**, *383*, 1−16.
(21) Gryta, M. Fouling in direct contact membrane distillation process. *J. Membr. Sci.* **2008**, *325*, 383−394.
(22) Suwal, S.; Doyen, A.; Bazinet, L. Characterization of protein, peptide and amino acid fouling on ion-exchange and filtration membranes: Review of current and recently developed methods. *J. Membr. Sci.* **2015**, *496*, 267−283.
(23) Young, A.; Venditti, S.; Berrueco, C.; Yang, M.; Waters, A.; Davies, H.; Hill, S.; Millan, M.; Crittenden, B. Characterization of crude oils and their fouling deposits using a batch stirred cell system. *Heat Transfer Eng.* **2011**, *32*, 216−227.
(24) Jonsson, G. R.; Lalot, S.; Palsson, O. P.; Desmet, B. Use of extended Kalman filtering in detecting fouling in heat exchangers. *Int. J. Heat Mass Transfer* **2007**, *50*, 2643−2655.
(25) Li, X.; Mo, Y.; Li, J.; Guo, W.; Ngo, H. H. In-situ monitoring techniques for membrane fouling and local filtration characteristics in hollow fiber membrane processes: A critical review. *J. Membr. Sci.* **2017**, *528*, 187−200.
(26) Ge, J.; Peng, Y.; Li, Z.; Chen, P.; Wang, S. Membrane fouling and wetting in a DCMD process for RO brine concentration. *Desalination* **2014**, *344*, 97−107.
(27) Charles, N.; Johnson, D. The occurrence and characterization of fouling during membrane evaporative cooling. *J. Membr. Sci.* **2008**, *319*, 44−53.
(28) Wallhäußer, E.; Hussein, M. A.; Becker, T. Detection methods of fouling in heat exchangers in the food industry. *Food Contr.* **2012**, *27*, 1−10.
(29) Wallhäußer, E.; Hussein, W. B.; Hussein, M. A.; Hinrichs, J.; Becker, T. Detection of dairy fouling: Combining ultrasonic measurements and classification methods. *Eng. Life Sci.* **2013**, *13*, 292−301.
(30) Wallhäußer, E.; Sayed, A.; Nöbel, S.; Hussein, M. A.; Hinrichs, J.; Becker, T. Determination of cleaning end of dairy protein fouling using an online system combining ultrasonic and classification methods. *Food Bioprocess Technol.* **2014**, *7*, 506−515.
(31) Virtanen, T.; Reinikainen, S.-P.; Kögler, M.; Mänttäri, M.; Viitala, T.; Kallioinen, M. Real-time fouling monitoring with Raman spectroscopy. *J. Membr. Sci.* **2017**, *525*, 312−319.
(32) Tun, C. M.; Fane, A. G.; Matheickal, J. T.; Sheikholeslami, R. Membrane distillation crystallization of concentrated salts-flux and crystal formation. *J. Membr. Sci.* **2005**, *257*, 144−155.
(33) Tachtatzis, C.; Sheridan, R.; Michie, C.; Atkinson, R. C.; Cleary, A.; Dziewierz, J.; Andonovic, I.; Briggs, N. E. B.; Florence, A. J.; Sefcik, J. Image-based monitoring for early detection of fouling in crystallisation processes. *Chem. Eng. Sci.* **2015**, *133*, 82−90.
(34) Lalot, S.; Desmet, B. The lock-in technique applied to heat exchangers: A semi-analytical approach and its application to fouling detection. *Appl. Therm. Eng.* **2017**, *114*, 154−162.
(35) Becheleni, E. M. A.; Borba, R. P.; Seckler, M. M.; Rocha, S. D. F. Water recovery from saline streams produced by electrodialysis. *Environ. Technol.* **2015**, *36*, 386−394.
(36) Wang, L.; Li, B.; Gao, X.; Wang, Q.; Lu, J.; Wang, Y.; Wang, S. Study of membrane fouling in cross-flow vacuum membrane distillation. *Sep. Purif. Technol.* **2014**, *122*, 133−143.
(37) Ho, J. S.; Sim, L. N.; Webster, R. D.; Viswanath, B.; Coster, H. G. L.; Fane, A. G. Monitoring fouling behavior of reverse osmosis membranes using electrical impedance spectroscopy: A field trial study. *Desalination* **2017**, *407*, 75−84.
(38) Gryta, M. Water desalination using membrane distillation with acidic stabilization of scaling layer thickness. *Desalination* **2015**, *365*, 160−166.
(39) Kimura, K.; Ogyu, R.; Miyoshi, T.; Watanabe, Y. Transition of major components in irreversible fouling of MBRs treating municipal wastewater. *Sep. Purif. Technol.* **2015**, *142*, 326−331.
(40) Tuladhar, T. R.; Paterson, W. R.; Macleod, N.; Wilson, D. I. Development of a novel non-contact proximity gauge for thickness measurement of soft deposits and its application in fouling studies. *Can. J. Chem. Eng.* **2000**, *78*, 935−947.
(41) Wang, S.; Wilson, D. I. Zero-discharge fluid-dynamic gauging for studying the swelling of soft solid layers. *Ind. Eng. Chem. Res.* **2015**, *54*, 7859−7870.
(42) Zan, C.; Shi, L.; Yang, W.; Ma, X. Evolution of composite fouling on a vertical stainless steel surface caused by treated sewage. *Front. Energy Power Eng. China* **2010**, *4*, 171−180.
(43) Lyster, E.; Kim, M.-m.; Au, J.; Cohen, Y. A method for evaluating antiscalant retardation of crystal nucleation and growth on RO membranes. *J. Membr. Sci.* **2010**, *364*, 122−131.
(44) Bartman, A. R.; Lyster, E.; Rallo, R.; Christofides, P. D.; Cohen, Y. Mineral scale monitoring for reverse osmosis desalination via real-time membrane surface image analysis. *Desalination* **2011**, *273*, 64−71.
(45) Phattaranawik, J.; Fane, A.; Wong, F. Novel membrane-based sensor for online membrane integrity monitoring. *J. Membr. Sci.* **2008**, *323*, 113−124.
(46) Thompson, J.; Rahardianto, A.; Kim, S.; Bilal, M.; Breckenridge, R.; Cohen, Y. Real-time direct detection of silica scaling on RO membranes. *J. Membr. Sci.* **2017**, *528*, 346−358.
(47) Lalot, S.; Pálsson, H. Detection of fouling in a cross-flow heat exchanger using a neural network based technique. *Int. J. Therm. Sci.* **2010**, *49*, 675−679.
(48) Pääkkönen, T. M.; Riihimäki, M.; Simonson, C. J.; Muurinen, E.; Keiski, R. L. Crystallization fouling of CaCO3 - Analysis of experimental thermal resistance and its uncertainty. *Int. J. Heat Mass Transfer* **2012**, *55*, 6927−6937.
(49) Crawford, R.; da Silva, A. K. Experimental testing of a passive, evaporation-based roof cooling system. *Energy Build.* **2014**, *71*, 12−19.
(50) Wallhäußer, E.; Hussein, W. B.; Hussein, M. A.; Hinrichs, J.; Becker, T. M. On the usage of acoustic properties combined with an artificial neural network—A new approach of determining presence of dairy fouling. *J. Food Eng.* **2011**, *103*, 449−456.
(51) Xu, X.; Li, J.; Li, H.; Cai, Y.; Cao, Y.; He, B.; Zhang, Y. Non-invasive monitoring of fouling in hollow fiber membrane via UTDR. *J. Membr. Sci.* **2009**, *326*, 103−110.
(52) Grafvonderschulenburg, D.; Vrouwenvelder, J.; Creber, S.; Vanloosdrecht, M.; Johns, M. Nuclear magnetic resonance microscopy studies of membrane biofouling. *J. Membr. Sci.* **2008**, *323*, 37−44.
(53) Gao, Y.; Haavisto, S.; Li, W.; Tang, C. Y.; Salmela, J.; Fane, A. G. Novel approach to characterizing the growth of a fouling layer during membrane filtration via optical coherence tomography. *Environ. Sci. Technol.* **2014**, *48*, 14273−14281.
(54) Feng, B.; Fang, Z.; Hou, J.; Ma, X.; Huang, Y.; Huang, L. Effects of heavy metal wastewater on the anoxic/aerobic-membrane bioreactor bioprocess and membrane fouling. *Bioresour. Technol.* **2013**, *142*, 32−38.
(55) Tijing, L. D.; Woo, Y. C.; Choi, J.-S.; Lee, S.; Kim, S.-H.; Shon, H. K. Fouling and its control in membrane distillation-A review. *J. Membr. Sci.* **2015**, *475*, 215−244.

DOI: 10.1021/acsomega.8b01058
ACS Omega 2018, 3, 17188−17198

(56) Zarebska, A.; Nieto, D. R.; Christensen, K. V.; Norddahl, B. Ammonia recovery from agricultural wastes by membrane distillation: Fouling characterization and mechanism. *Water Res.* **2014**, *56*, 1−10.
(57) Zhao, Z.-P.; Xu, L.; Shang, X.; Chen, K. Water regeneration from human urine by vacuum membrane distillation and analysis of membrane fouling characteristics. *Sep. Purif. Technol.* **2013**, *118*, 369−376.
(58) Naidu, G.; Jeong, S.; Vigneswaran, S.; Hwang, T.-M.; Choi, Y.-J.; Kim, S.-H. A review on fouling of membrane distillation. *Desalin. Water Treat.* **2015**, *57*, 10052−10076.
(59) Tian, L.; Chen, X. D.; Yang, Q. P.; Chen, J. C.; Shi, L.; Li, Q. Effect of calcium ions on the evolution of biofouling by Bacillus subtilis in plate heat exchangers simulating the heat pump system used with treated sewage in the 2008 Olympic Village. *Colloids Surf., B* **2012**, *94*, 309−316.
(60) Sioutopoulos, D. C.; Karabelas, A. J. Evolution of organic gel fouling resistance in constant pressure and constant flux dead-end ultrafiltration: Differences and similarities. *J. Membr. Sci.* **2016**, *511*, 265−277.
(61) Li, W.; Liu, X.; Wang, Y.-N.; Chong, T. H.; Tang, C. Y.; Fane, A. G. Analyzing the evolution of membrane fouling via a novel method based on 3D optical coherence tomography imaging. *Environ. Sci. Technol.* **2016**, *50*, 6930−6939.
(62) Xu, Q.; Ye, Y.; Chen, V.; Wen, X. Evaluation of fouling formation and evolution on hollow fibre membrane: Effects of ageing and chemical exposure on biofoulant. *Water Res.* **2015**, *68*, 182−193.
(63) Woods, J. Membrane processes for heating, ventilation, and air conditioning. *Renew. Sustain. Energy Rev.* **2014**, *33*, 290−304.
(64) Zhang, L.-Z. Progress on heat and moisture recovery with membranes: From fundamentals to engineering applications. *Energy Convers. Manage.* **2012**, *63*, 173−195.
(65) Pérez-Lombard, L.; Ortiz, J.; Pout, C. A review on buildings energy consumption information. *Energy Build.* **2008**, *40*, 394−398.
(66) Ge, G.; Abdel-Salam, M. R. H.; Besant, R. W.; Simonson, C. J. Research and applications of liquid-to-air membrane energy exchangers in building HVAC systems at University of Saskatchewan: A review. *Renew. Sustain. Energy Rev.* **2013**, *26*, 464−479.
(67) Abdel-Salam, M. R. H.; Ge, G.; Fauchoux, M.; Besant, R. W.; Simonson, C. J. State-of-the-art in liquid-to-air membrane energy exchangers (LAMEEs): A comprehensive review. *Renew. Sustain. Energy Rev.* **2014**, *39*, 700−728.
(68) Abdel-Salam, M. R. H.; Fauchoux, M.; Ge, G.; Besant, R. W.; Simonson, C. J. Expected energy and economic benefits, and environmental impacts for liquid-to-air membrane energy exchangers (LAMEEs) in HVAC systems: A review. *Appl. Energy* **2014**, *127*, 202−218.
(69) Olufade, A. O.; Simonson, C. J. Detection of crystallization fouling in a liquid-to-air membrane energy exchanger. *Exp. Therm. Fluid Sci.* **2018**, *92*, 33−45.
(70) Bott, T. R. Aspects of crystallization fouling. *Exp. Therm. Fluid Sci.* **1997**, *14*, 356−360.
(71) Briançon, S.; Colson, D.; Klein, J. P. Experimental study and theoretical approach of cooling surfaces fouling in industrial crystallizers. *Chem. Eng. Res. Des.* **1997**, *75*, 147−151.
(72) Pääkkönen, T. M.; Riihimäki, M.; Simonson, C. J.; Muurinen, E.; Keiski, R. L. Modeling $CaCO_3$ crystallization fouling on a heat exchanger surface - Definition of fouling layer properties and model parameters. *Int. J. Heat Mass Transfer* **2015**, *83*, 84−98.
(73) Walker, P.; Sheikholeslami, R. Assessment of the effect of velocity and residence time in CaSO4 precipitating flow reaction. *Chem. Eng. Sci.* **2003**, *58*, 3807−3816.
(74) Augustin, W.; Bohnet, M. Influence of the ratio of free hydrogen ions on crystallization fouling. *Chem. Eng. Process.* **1995**, *34*, 79−85.
(75) Mullin, J. W. *Crystallization*, 4th ed.; Reed Educational and Professional Publishing Ltd: Oxford, England, 2001.
(76) Bansal, B.; Chen, X. D.; Müller-Steinhagen, H. Analysis of "classical" deposition rate law for crystallisation fouling. *Chem. Eng. Process.* **2008**, *47*, 1201−1210.
(77) Bott, T. R. Crystallisation and Scale Formation. *Fouling of heat exchangers*; Elsevier Science: Amsterdam, Netherlands, 1995; pp 97−103.
(78) Rodríguez-hornedo, N.; Murphy, D. Significance of controlling crystallization mechanisms and kinetics in pharmaceutical systems. *J. Pharm. Sci.* **1999**, *88*, 651−660.
(79) Mwaba, M. G.; Rindt, C. C. M.; Van Steenhoven, A. A.; Vorstman, M. A. G. Experimental Investigation of CaSO4Crystallization on a Flat Plate. *Heat Transfer Eng.* **2006**, *27*, 42−54.
(80) Olufade, A. O.; Simonson, C. J. Application of indirect non-invasive methods to detect the onset of crystallization fouling in a liquid-to-air membrane energy exchanger. *Int. J. Heat Mass Transfer* **2018**, *127*, 663−673.
(81) Huang, S.-M.; Zhang, L.-Z. Researches and trends in membrane-based liquid desiccant air dehumidification. *Renew. Sustain. Energy Rev.* **2013**, *28*, 425−440.
(82) Beriault, D. A. *Run-Around Membrane Energy Exchanger Prototype 4 Design and Laboratory Testing*, MSc Thesis, University of Saskatchewan: Saskatoon, SK, 2011.
(83) ZEISS Germany. *ZEN 2 Core: Imaging Software for Connected Microscopy in Material Laboratories*. https://www.zeiss.com/microscopy/int/products/microscope-software/zen-2-core.html (accessed Aug 19, 2017).
(84) Egerton, R. F. *Physical Principles of Electron Microscopy: An Introduction to TEM, SEM, and AEM*, 2nd ed.; Springer International Publishing Switzerland: Edmonton, Canada, 2016.
(85) Agron, P. A.; Busing, W. R. Magnesium dichloride hexahydrate, MgCl2.6H2O, by neutron diffraction. *Acta Crystallogr., Sect. C: Cryst. Struct. Commun.* **1985**, *41*, 8−10.
(86) Song, Y.; Shan, D.; Chen, R.; Zhang, F.; Han, E.-H. Formation mechanism of phosphate conversion film on Mg-8.8Li alloy. *Corros. Sci.* **2009**, *51*, 62−69.
(87) Hristovski, K.; Westerhoff, P.; Crittenden, J. An approach for evaluating nanomaterials for use as packed bed adsorber media: A case study of arsenate removal by titanate nanofibers. *J. Hazard. Mater.* **2008**, *156*, 604−611.

DOI: 10.1021/acsomega.8b01058
ACS Omega 2018, 3, 17188−17198